NANOSYSTEMS: PHYSICS, CHEMISTRY, MATHEMATICS, 2013, 4 (3), P. 395–404

EFFECT OF Li+ CO-DOPING ON THE LUMINESCENCE PROPERTIES OF ZnO:Tb^{3+} NANOPHOSPHORS

Partha P. Pal[1], J. Manam

[1]Deptartment of Applied Physics, Indian School of Mines, Dhanbad-826004, India

phys.ppal@gmail.com, jairam_manam@yahoo.co.in

PACS 78.67.Qa, 78.55.Et

Li^+ co-doped ZnO:Tb^{3+} nanocrystals were synthesized via the chemical co-precipitation method in order to study the effect of Li^+ co-doping. The samples were characterized by means of SEM, XRD, FTIR, Reflectance, PL and TL studies. SEM images showed that the samples were composed of nanorods with diameters of 50 to 90 nm and lengths of approximately 600 nm to 1.3 μm. XRD analysis revealed pure phase of ZnO with hexagonal wurtzite structure. XRD study also showed no change in the peak pattern for Li^+ co-doping; a slight shift of the (101) peaks towards lower angle can be seen. Sample crystal sizes were found to be in the 10–25 nm range. Photoluminescence intensity was enhanced due to a minute amount of Li^+ co-doping in the sample. The X-induced thermoluminescence gave a glow peak at 320 °C for the Li^+ co-doped sample, which was shifted to a lower temperature and had twice the intensity of the ZnO:Tb^{3+} sample.

Keywords: terbium, rare-earth, lithium, photoluminescence, thermoluminescence, zinc oxide.

1. Introduction

Rare earth doped ZnO has been the subject of interest over the last few years. Recently, nanocrystalline ZnO has been synthesized in various shapes, like nanorods, nanospheres, nanoflowers etc. while being doped with rare-earth (RE) ions to obtain enhanced luminescence properties. These qualities make the aforementioned structures useful in in various optoelectronic devices like vacuum fluorescent display (VFD), field emission display (FED) and electroluminescent display (ELD) etc [1–5]. The intra-shell transition between the 4f shells of the RE ions make their luminescence properties very attractive. Doping RE ions into the ZnO matrix is very difficult because, firstly, the ionic radii of RE ions (e.g. Tb^{3+} ∼0.92Å) are much larger than that of Zn^{2+} ions (∼0.74Å) and secondly substitution creates a charge imbalance, as RE^{3+} ions (Charge: +3) substitutes the Zn^{2+} sites (Charge: +2) in the ZnO host matrix. The charge compensation from the local defect sites results in lattice deformation, which is not desired. It would be much more convenient to provide a charge compensating material for the formation of a stable compound. The alkali metals like Na, K, Li etc. are the most suitable candidates in this regard.

In the case of high temperature treatment, the luminescence efficiency of rare-earth materials is often found to decrease due to self-quenching. That is why room temperature synthetic methods, like precipitation method, sol-gel method, etc. are considered very convenient methods for rare-earth doping. Terbium (Tb) is a very interesting rare-earth element known for its bright green emissions due to Tb^{3+} related peaks at 490 nm ($^5D_4 \rightarrow {}^7F_6$) and 544 nm ($^5D_4 \rightarrow {}^7F_5$) and thus, very suitable for doping in ZnO; because that oxide is itself a green emitting phosphor and generally gives broad green (532 nm) and blue-green (450 nm, 472 nm) emissions. Earlier studies showed that a small amount

of Li^+ doping enhanced the luminescence efficiency [6] due to charge compensations and the creation of defects and traps. It is expected that with a minute amount of Li^+ co-doping, the green photoluminescence (PL) and thermoluminescence (TL) emissions will be enhanced.

In this work, undoped ZnO, ZnO:Tb^{3+} and Li^+ co-doped ZnO:Tb^{3+}, were synthesized successfully by the co-precipitation method. The optical properties of these samples were systematically studied by UV-Vis Diffuse reflectance (DR), thermoluminescence (TL) and photoluminescence (PL) separately, whereas the structural properties were carried out by X-ray diffraction (XRD), scanning electron microscopy (SEM) and Fourier transform infrared spectroscopy (FTIR). The effects of Li^+ co-doping on its different properties were followed, observed, described and explained.

2. Experimental

Undoped, Tb^{3+} doped and Li^+ co-doped ZnO were prepared by the co-precipitation method. The undoped ZnO sample was prepared by mixing equal volumes of 0.05 *M* ethanolic $ZnCl_2$ solution with 0.20 *M* ethanolic NaOH at room temperature. Firstly, suitable amounts of $ZnCl_2$ and NaOH were separately dissolved in ethanol to prepare 0.05 *M* $ZnCl_2$ and 0.20 *M* NaOH solutions at room temperature. Then, the two solutions were mixed and magnetically stirred for 6 hours at room temperature. During this process, NaOH reacts with $ZnCl_2$ to form ZnO. The mixed sample was then filtered with a 125 mm Whiteman-42 filter paper. After complete filtration, the residue on the paper was collected and dried. The filtrand was then washed in ethanol and dried at 80 °C to provide a favorable temperature for nanorod formation. For co-doping Li^+ and Tb^{3+} ions, the requisite amounts of LiCl and $TbCl_3$ [Sigma-Aldrich, 99.9%] were added before mixing the 0.05 *M* $ZnCl_2$ and 0.20 *M* NaOH solutions. After drying and collecting, the samples were annealed at 200 °C for two hours.

The powder sample was characterized over a wide range of Bragg angles 2θ ($10^\circ \leqslant 2\theta \leqslant 80^\circ$) with a Bruker D8 Focus XRD instrument with a Cu target (K_α=1.5406 Å) at a scanning rate of 2° per min. The FTIR spectrum (KBr pellet) was taken from 400 to 4000 cm^{-1} on a 'FTIR Spectrum RX I', (Perkin Elmer, Switzerland) spectrometer. The SEM image was taken with Hitachi S 3400-N Scanning Electron microscope. The differential scanning calorimetry (DSC) analysis was carried out using a Perkin Elmer DSC7 Differential Scanning Calorimeter. PL emission and excitation studies were carried out by a commercially available personal computer-based Hitachi FL 2500 Fluorescence spectrophotometer with a 150W xenon lamp over the wavelength range 350 to 700 nm. Thermoluminescence studies were carried out by using a personal computer-based Thermoluminescence Analyzer System (TL 1007) supplied by Nucleonix Systems private ltd. India.

3. Results and Discussion

3.1. SEM Studies

Fig.1 (a) and (b) shows the particle morphologies of ZnO:$Tb^{3+}$and 1wt% Li^+ co-doped ZnO:Tb^{3+} nanophosphors. As can be seen, the particles are composed of nanorods and nanoparticles. In the case of ZnO:Tb^{3+} sample, the diameters and length of the nanorods were found to range from 70 to 90 nm and 800 nm to 1.3 μm respectively, whereas from the image of the Li^+ co-doped ZnO:Tb^{3+}, it is clear that there is loss of sample crystallinity due to the oxygen vacancy brought about by Li^+ ion incorporation

[7, 8]. Here, the diameters and lengths of most nanorods were found to range from 50 to 70 nm and 600 nm to 800 nm respectively, which were less than that of the ZnO:Tb^{3+} sample. Due to the Li^+ ion, the growth of nanocrystals was found to be suppressed here and nanorods were partially formed, although some of the nanorods in this case were also found to be more than 1 μm in length. The formation of these morphologies can be attributed to the supersaturation of ZnO nuclei [9]. Nanorod growth begins when both Zn^{2+} and OH^- ions reach supersaturated levels. The PH value in the solution plays a vital role in this regard.

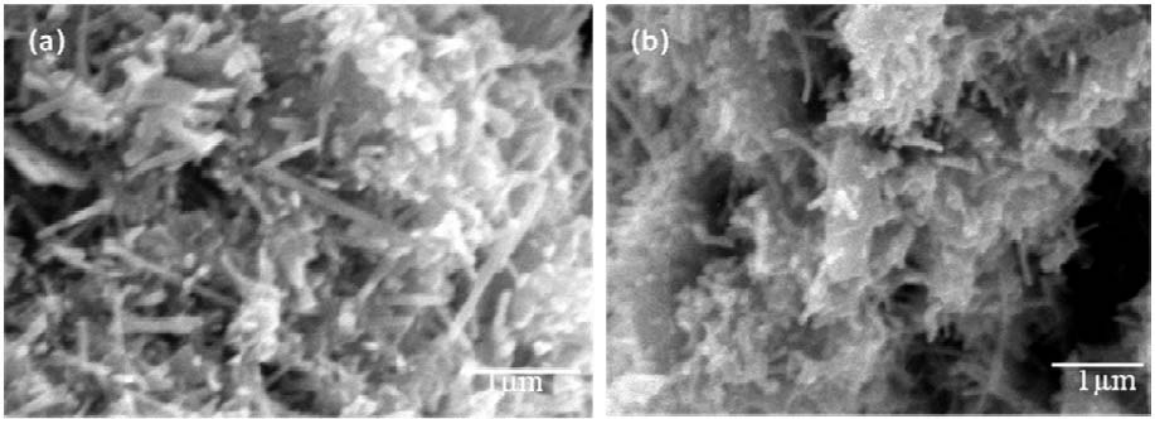

Fig. 1. SEM image for the (a) ZnO:Tb^{3+} and (b) 1wt% Li co-doped ZnO:Tb^{3+} nanorods

3.2. XRD Studies

The room temperature XRD patterns of the undoped, ZnO:Tb^{3+} and Li^+ co-doped ZnO:Tb^{3+} powder samples are shown in Figure 2. The XRD study was done over a wide range of Bragg angles (20 ° – 80 °). The XRD pattern of all the samples showed ZnO hexagonal wurtzite structure. The peaks were well matched with the JCPDS data card No. 79-0206. The data with particle sizes are shown in Table 1. The grain size of ZnO:Tb^{3+} calculated by the Debye-Scherrer formula was found to be in the 10–25 nm range. The XRD study showed no change in the XRD peak pattern, confirming that Li^+ ions were well incorporated in the crystal lattice. In all likelihood, the slight shift of the (101) peak towards lower angle seen for the Li^+ co-doped sample may indicate an increase in the lattice parameters due to Li^+ doping. This increase in lattice parameters is due to lattice distortion as Li^+ ions occupy the lattice sites [10]. The crystal sizes in the sample were calculated by the Debye-Scherrer formula:

$$D = 0.9\lambda/\beta cos\theta$$

where β is the full-width at half-maximum (FWHM), and λ is the wavelength of the X-Ray used. The wavelength of the X-Ray used here is K_α=1.5406Å (Cu target). The crystal sizes were calculated to be in the of 15 to 20 nm range for Li^+ co-doped ZnO:Tb^{3+} and 20 to 30 nm for ZnO:Tb^{3+}.

3.3. FTIR Studies

The 'FTIR' spectra of the undoped ZnO, Tb^{3+} doped ZnO and Li^+ co-doped ZnO:Tb^{3+} were also studied systematically and the results are shown in Fig. 3. The FTIR spectra of the undoped ZnO sample consisted of four large absorption bands. The

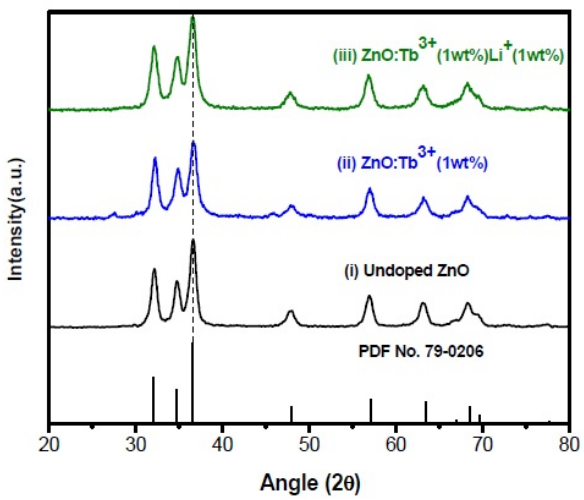

Fig. 2. Room temperature XRD pattern (i) undoped ZnO, (ii) ZnO:Tb^{3+} (1wt%), (iii) Li^{+} (1wt%) co-doped ZnO:Tb^{3+} (1.0 wt%) along with the standard XRD peaks for ZnO (JCPDS No. 79-0206)

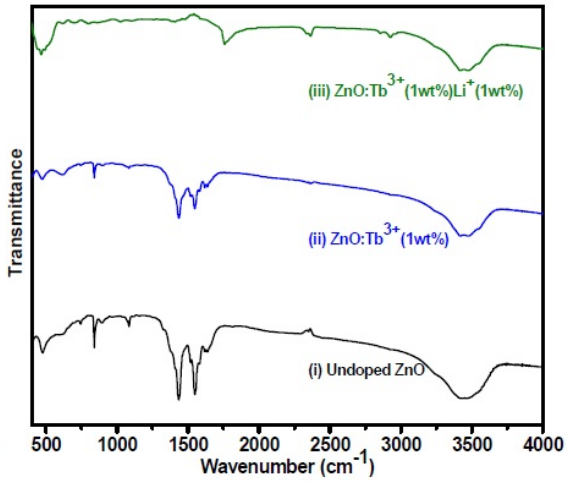

Fig. 3. FTIR spectra of the (i) as synthesized ZnO, (ii) annealed ZnO and (iii) annealed ZnO:Tb^{3+} (1wt%) nanorods

Table 1. Comparison of the experimental and reference values [PDF no. −79−0206] of XRD peak Positions and d-spacings of Li^{+} co-doped ZnO:Tb^{3+} sample. The crystal sizes are indicated corresponding to each peak

Peak position (2θ exp.)	Peak position (2θ ref.)	d spacing exp. [Å]	d spacing ref. [Å]	Particle Size (nm)	h	k	l	Relative Intensity (%)
32.214	31.768	2.7765	2.8145	18.14	1	0	0	52.4
34.890	34.422	2.5694	2.6032	17.87	0	0	2	49.4
36.584	36.253	2.4543	2.4759	20.72	1	0	1	80.7
47.859	47.540	1.8991	1.9111	16.58	1	0	2	17.9
56.926	56.594	1.6162	1.6249	18.96	1	1	0	25.8
63.114	62.858	1.4818	1.4772	16.12	1	0	3	28.2
66.233	66.374	1.4099	1.4072	19.53	2	0	0	8.3
68.305	67.947	1.3802	1.3784	18.65	1	1	2	42.6
69.931	69.875	1.3607	1.3585	16.31	2	0	1	20.2

large band at 475 cm^{-1} was attributed to the Zn-O stretching in the ZnO lattice. Two others bands locating at 1545 and 1431 cm^{-1} were attributed to asymmetric and symmetric C=O stretching vibration modes. The presence of C=O may be due to the atmospheric CO_2. The wide absorption band at 3438 cm^{-1} corresponds to the stretching mode of OH group [11]. These bands were present in both the Tb^{3+}-doped and Li^+ co-doped ZnO:Tb^{3+} samples. There was no change in the Zn-O and -OH peak positions due to the Li^+, but the peak for Zn-O stretching was found to be more prominent for the Li^+ co-doped sample and there was a shift for C=O peak. An increase in peak sharpness was also noted, indicating a better crystal quality for the Li^+ doping. The corresponding peak positions are shown in Table 2. Also the FTIR study showed that the samples were free from any other organic impurities and suitable for the PL and TL studies.

Table 2. Assignment of FTIR bands of Undoped, 1wt% $Tb^{3+}$and 1wt% Li co-doped Tb^{3+} doped ZnO nanocrystals

Samples	ZnO Stretching mode (cm^{-1})	OH stretching mode (cm^{-1})	C=O stretching modes (cm^{-1})	CO_2 Mode (cm^{-1})
Undoped ZnO	474	3440	1439, 1542	2351 2351
ZnO:Tb^{3+}(1wt%)	470	3420	1437 1503	2369
Li^+ (1wt%) co-doped ZnO:Tb^{3+}(1wt%)	440	3422	1391 1517	2378

3.4. DSC analysis

The Differential Scanning Calorimetric analysis of the Tb^{3+} doped ZnO sample is shown in fig. 4. Though the DSC curve did not show much variation after the initial rise at 30 ° C, it showed a fall up to 200 ° C. This may be due to the weight loss of the samples for the removal of water. The exothermic rise at 330 ° C may be due to the crystallization of wurtzite ZnO structure [12]. The endothermic broad peaks of the curve near 355 ° C may be due to the auto combustion reaction or possibly the removal of other organic compounds which were attached during sample preparation but not removed during washing. The peak after 500 ° C showed no significant weight loss, indicating that the sample was crystalline in nature.

3.5. UV-Vis Diffuse Reflectance Studies

Fig. 5 represents the diffuse reflectance (DR) spectra of the undoped ZnO:$Tb^{3+}$and 1wt% Li^+ co-doped ZnO:Tb^{3+} samples. In all cases, two absorption edges were observed; near 350 nm and 235 nm. The absorption edge of the Li^+ co-doped sample was found to have red shifted. Earlier, a significant change in the crystallinity and particle size was observed, and now, a clear red-shift of the absorption edge was seen due to the introduction of Li^+ ions into ZnO:Tb^{3+}. This occurred because, when Zn^{2+} sites were occupied by Li^+ ion, there was an increase of oxygen vacancies, which changed the energy band structure resulting in a narrowing of the band gap and subsequently shifting of the absorption edge to a higher wavelength [13]. Meanwhile, the reflectance of ZnO:Tb^{3+} sample has a blue-shift followed by bandgap widening due to the increase of Fermi level because of doping with rare-earth ions. The reflectance intensity, in the case of the Li^+ co-doped sample,

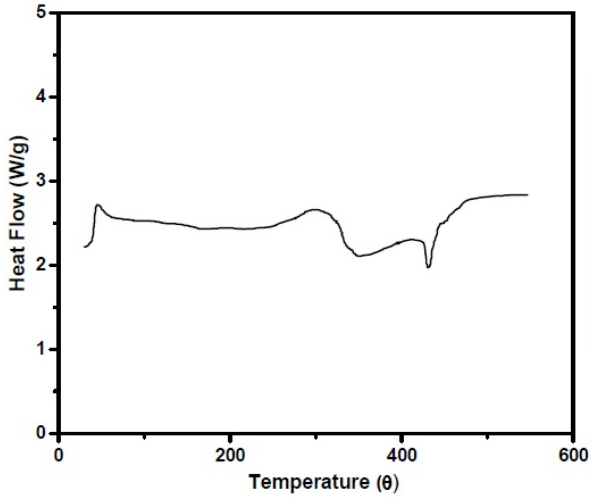

Fig. 4. DSC curves for Tb^{3+} doped ZnO nanocrystals

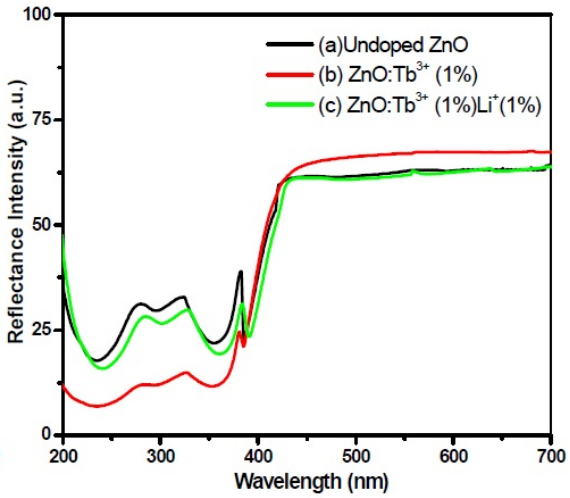

Fig. 5. Room temperature diffuse reflectance of the (a) Undoped (b) 1wt% Tb3+ and (c) 1wt% Li co-doped Tb3+ doped ZnO nanocrystals

was found decreased, which is an effect of crystallinity loss due to the oxygen vacancy. Conversely, the reflectance intensity was found to increase in the ZnO:Tb^{3+} sample, which may result from the Fermi level increase due to the presence of rare-earth ions [14].

The bandgaps of undoped ZnO, Tb^{3+} doped ZnO and Li^{+} co-doped ZnO:Tb^{3+} samples were calculated from the reflectance study (Fig. 6) using the Kubelka-Munk function, which is a function equivalent to the absorption coefficient and is denoted by:

$$F(R_\alpha) = (1 - R_\alpha)^2 / 2R_\alpha$$

where R_α is the reflectance intensity. More accurately, R_α is the reflectance of an infinitely thick sample with respect to a reference at each wavelength [15]. The square of the function multiplied by $h\nu$ i.e $[F(R_\alpha)h\nu]^2$ were plotted against photon energy $h\nu$. The intercept of the slope of the graph at x-axis gave the required bandgap. The plotted graphs are shown fig. 5. The bandgap energies calculated here had values of 3.22±0.01 eV, 3.23±0.01 eV, 3.21±0.01 eV for undoped ZnO, Tb^{3+} doped ZnO and Li^{+} co-doped ZnO:Tb^{3+} respectively. The bandgap values decreased due to Li^{+} co-doping, whereas the value increased for the rare-earth doped sample, which is a consequence of the reasons described above.

The bandgap values for doped compounds were much lower than that of bulk pure ZnO (3.37 eV). This was due to the presence of a single crystal in the sample [16].

3.6. Photoluminescence Studies

The room temperature photoluminescence spectra of the Li^{+} co-doped ZnO:Tb^{3+} and ZnO:Tb^{3+} sample are shown in Figure 7. Fig 7 (I) shows the PL emission spectra of the Li^{+} co-doped ZnO:Tb^{3+}, ZnO:Tb^{3+} and the undoped ZnO sample. The photoluminescence intensity increased due to the inclusion of Li^{+}. While all samples gave a broad blue peak near 435 nm due to the host lattice, the Tb^{3+}-doped sample showed a blue-green emission peak near 534 nm, which was due to the transition $^5D_4 \rightarrow ^7F_5$ in Tb^{3+} ions [17]. The peak for this transition was found to be more prominent and intense

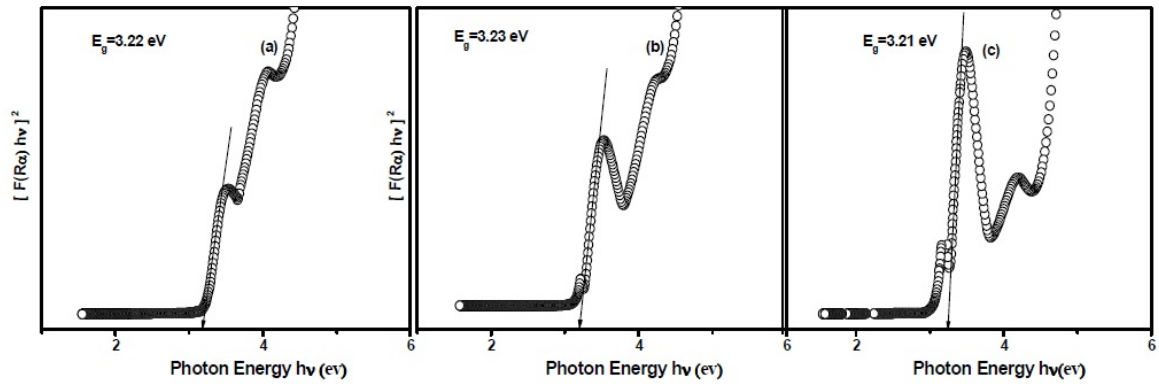

Fig. 6. Plot for $[F(R\alpha)h\nu]^2$ as a function of the incident photon energy ($h\nu$) for the (a) Undoped (b) 1wt% Tb^{3+} and (c) 1wt% Li co-doped Tb^{3+} doped ZnO nanocrystals

in the Li^+ co-doped sample at 554 nm. The corresponding excitation spectra are shown in Fig. 7 (I), providing confirmation of the above study. The charge compensation by the Li^+ ions provided chemical stability, and the improved crystal quality had a great influence on the enhancement of PL peak intensities in the Li^+ co-doped sample. One must keep in mind that excess Li^+ brings excess oxygen vacancies, which leads to more luminescence quenching. So, Li^+ should always be present in lower concentration than the rare-earth ion, which is sufficient for charge compensation and thus producing high luminescence.

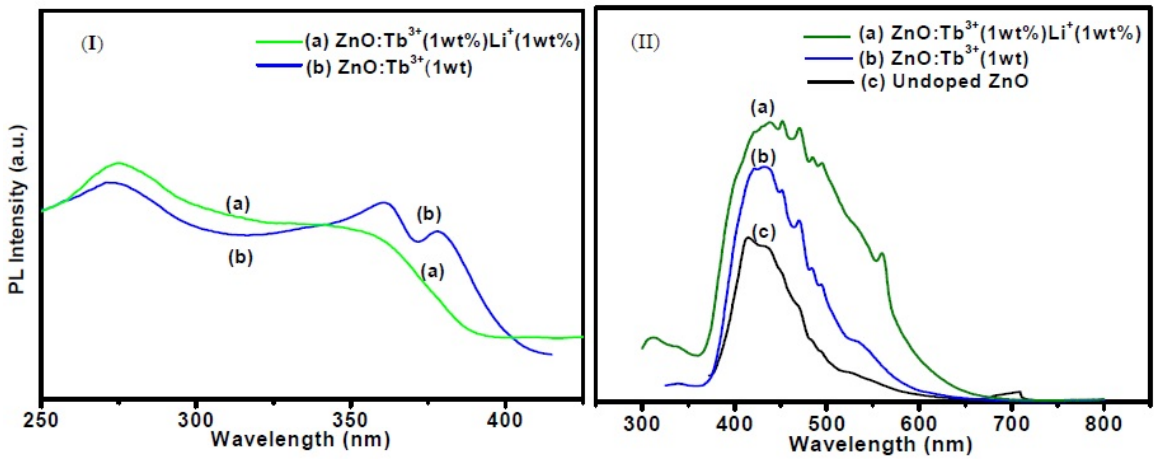

Fig. 7. Room temperature (I) excitation spectra of the (a) Li^+ codoped ZnO:Tb^{3+} and (b) Tb^{3+} doped ZnO at E_x=540 nm and (II) emission spectra of the (a) Li^+ co-doped ZnO:Tb^{3+} (b) Tb^{3+} doped ZnO and (c) undoped ZnO sample at Em=275 nm

3.7. Thermoluminescence Studies

The thermoluminescence study of the co-doped, RE doped and undoped samples were carried out at temperatures ranging from 27–400 °C. Fig. 8 shows the TL glow curves of the undoped, Tb^{3+} doped and Li^+ co-doped ZnO:Tb^{3+} samples. The Li^+ co-doped sample showed an intense peak at 320 °C, while the Tb^{3+}-doped sample gave a shifted peak at 355 °C. The undoped sample showed peak at 185 °C. The TL intensity of

the Li^+ co-doped sample was found to be almost twice that of the ZnO:Tb^{3+} sample. This showed that the inclusion of Li^+ ion in the lattice increased the TL intensity by about two orders of magnitude more than that of the ordinary Tb^{3+} doped sample. Co-doping the ZnO:Tb^{3+} with Li^+ not only shifted the TL peak to lower temperatures, but also appeared to enhance the intensity of that peak [18]. This enhancement of the TL peak arising from Li^+ doping can be attributed to the formation of traps. In the case of TL, the traps are responsible for the glow curves. Due to the high energy X-ray irradiation, traps are formed in the lattice and charge carriers, released by the dopant ions, remain in those traps. Then, on thermal stimulation, these trapped charge carriers are released, which then recombine with their counterpart i.e. electrons recombine with the holes to produce energy for luminescence. In case of first order kinetics, there is negligible re-trapping and recombination is in dominant, however in the case of second order kinetics, retrapping dominates. The glow peaks were found to be of anti symmetric nature in first order kinetics, viz. the glow peaks for both Li^+ co-doped ZnO and ZnO:Tb^{3+} were found to be antisymmetric in nature. Whereas, the second order glow peaks are more symmetric in nature viz. the glow peak of undoped ZnO observed here.

3.8. Role of Li^+ in defect formation

The paper discusses the effect of the charge compensating Li^+ ion on the luminescence properties of rare-earth (Tb^{3+}) activated ZnO. For luminescence phenomena, defect formation plays a key role. Previous studies have shown that a small amount of Li^+ doping resulted in increased luminescence intensity when the concentration of Li^+ ion was much less compared to the corresponding rare-earth ions. This may be due to the increase of lattice energy caused by the addition of Li^+ ions [19]. To minimize this lattice energy, Tb^{3+} ions were distributed uniformly in the lattice due to which the PL intensity was enhanced [20, 21]. In the case of high Li^+ ion concentration, many lattice defects may be induced, which is also not suitable for photoluminescence; thus decreasing the PL intensities of the phosphors. For luminescence to occur, electron-hole pair recombination is necessary, and in this case, the Li^+ ion has a role in the transfer of the electron between the following: the surface level and the Tb^{3+} ion; the hole transfer between the valence band and the Tb^{3+} ion; the electron transfer between the conduction band and the surface level; and the transition probabilities between the 4f levels [22]. The broad green PL emission from ZnO may also be affected by both Li^+ and Tb^{3+} incorporation. Under reducing conditions, Li^+ insertion leads to a series of shallow donor levels. Also, the Li^+ ions invite oxygen vacancies, thus increasing lattice distortion. The Li^+ ions leads to series of energy levels near the conduction band. The recombination of the intrinsic shallow donors in the conduction band causes the green emission in ZnO, however, for Li^+ co-doped ZnO:Tb^{3+} the green emission was due to the recombination of the shallow donors created by the impurities like the interstitial Li^+. Earlier studies showed that due to the rare-earth activator (Tb^{3+}) and the charge compensator (Li^+), the lifetime of the green emission was increased, which indicates that the electrons remained trapped inside the shallow donor levels. These electrons were then released with the radiation to recombine with the holes which were trapped earlier by the defects, e.g. oxygen vacancies. This phenomenon is similar to the thermoluminescence discussed above.

4. Conclusions

ZnO:Tb^{3+} nanoparticles were co-doped with Li^+ by the precipitation method using ethanol as solvent and the effect this co-doping had on the luminescence properties were

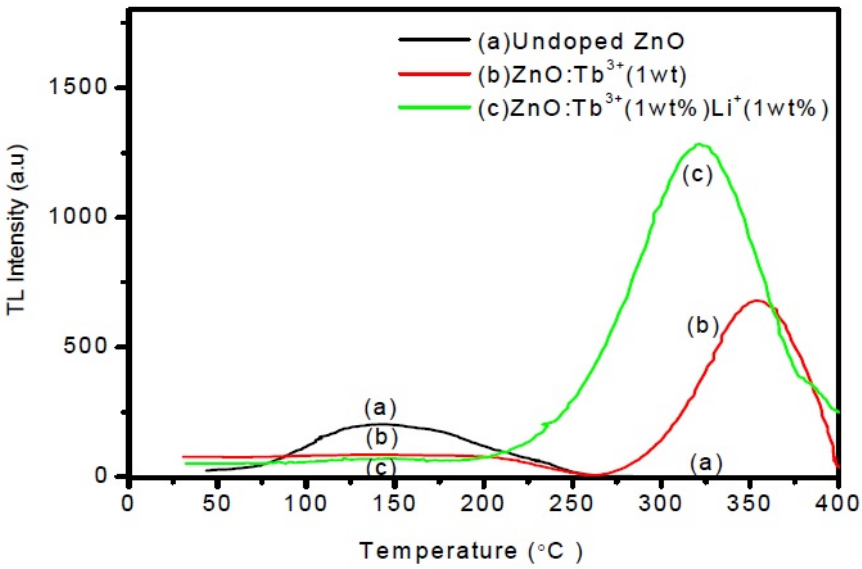

Fig. 8. X-irradiated TSL glow curve for Li^+ co-doped ZnO, ZnO:Tb^{3+} and undoped ZnO irradiated for 5 mins

discussed. SEM image showed the formation of nanorods and the FTIR study showed that the samples were suitable for PL and TL studies. XRD study revealed no impure phase due to Li^+ doping; it was found that Li^+ ion can influence the lattice parameters. Both the PL and TL peak intensities were improved due to charge compensation by the Li^+ ions. The TL glow peak was found to be shifted to a lower temperature than that of the rare-earth doped sample without Li^+ co-doping, which showed that the sample can be readily used in display devices and thermal sensors. In brief, a minute amount of Li^+ co-doping on rare-earth doped ZnO nanorods was very effective at improving its luminescence properties.

Acknowledgements

One of the authors, Pal gratefully acknowledges the ISM research fellowship by Govt. of India. The authors are thankful to Dr. S. K. Sharma, Prof. A. Sarkar, Dr. N. M. Mishra for PL, FTIR and DSC studies.

References

[1] Nakanishi Y., Miyake A., Kominami H., Aoki T., Hatanaka Y., Shimaok G. Preparation of ZnO thin films for high-resolution field emission display by electron beam evaporation. *Appl. Surf. Sci.* **142**, P. 233–236 (1999).
[2] Huang M.H.,Mao S., Feick H., Room temperature ultraviolet nanowire nanolasers. *Science*, **292**, P. 1897–1899 (2001).
[3] Zhang J.,Feng H., Hao W.,Wang T. Luminescence of nanosized ZnO/polyaniline films prepared by self-assembly. *Ceramics International*, **33**, P. 785–788 (20070.
[4] Hellemans A., Laser Light From a Handful of Dust. *Science*, **284**, P. 24–25 (1999).
[5] Yi L., Hou Y., Zhao H. Photo- and electro-luminescence properties of ZnO: Zn thin film. *Displays*, **21**, P. 147–149 (2000).
[6] Prokić M. Development of highly sensitive $CaSO_4$: Dy/Tm and MgB_4O_7 : Dy/Tm sintered thermoluminescent dosimeters. *Nucl. Inst. Meth.*, **175**(1), P. 83–86 (1980).
[7] Y. Wu, Y. Wang, D. He, M. Fu, Z. Chen and Y.Li. Spherical Zn_2SiO_4:Eu^{3+}@SiO_2 phosphor particles in coreshell structure: Synthesis and characterization. *J. Lumin.*, **130**, P. 1768 (2010).

[8] H. Liu, Y. Hao, H. Wang, J. Zhao, P. Huang and B. Xu. *J. Lumin.*, **131**, P. 2422 (2011).
[9] Sreekantan S., Gee L.R., Lockman Z. Room temperature anodic deposition and shape control of one-dimensional nanostructured zinc oxide. *J.Alloys and Comp.*, **476**, P. 513 (2009).
[10] Sun L., Qian C., Liao C.,Wang X., Yan C. Luminescent properties of Li^+ doped nanosized Y_2O_3:Eu *Solid State Commun.*, **119**, P. 393 (2001).
[11] Maensiri S.,Laokul P., Promarak V. Synthesis and optical properties of nanocrystalline ZnO powders by a simple method using zinc acetate dihydrate and poly(vinyl pyrrolidone) *J. Cryst. Growth*, **289**, P. 102 (2006).
[12] Majumder S.B., Jain M., Dobal P.S., Katiyar R.S., Investigations on solution derived aluminium doped zinc oxide thin films. *Materials Science and Engineering B*, **103**, P. 16–25 (2003).
[13] Maa Q., Zhou Y., Zhang A., Lu M., Zhou G., Li C. Synthesis and optical properties of novel red phosphors $YNbTiO_6$:Eu^{3+} with highly enhanced brightness by Li^+ doping. *Solid State Sci.* **11**, P. 1124–1130 (2009).
[14] Burstein E., Anomalous Optical absorption limit in in Sb, *Phys. Rev.* **93**, P. 632 (1954).
[15] Tiekun Jia,WeiminWang, Fei Long, Zhengyi Fu, HaoWang, Qingjie Zhang, Fabrication, characterization and photocatalytic activity of La-doped ZnO nanowires. *J.Alloy.Compd.*, **484**, P. 410 (2009).
[16] Srikant V., Clarke D.R., On the optical band gap of zinc oxide. *J. Appl. Phys.*, **83**, P. 5447 (1998).
[17] Zhang J.,Feng H., Hao W.,Wang T. Luminescent properties of ZnO sol and film doped with Tb^{3+} ion. *Mat. Sci. Eng. A*, **425**, P. 346–348 (2006).
[18] Rojas S.S., Yukimitu K., De Camargo A.S.S., Nunes L.A.O.,.Hernandes A.C. *J. Non-Cryst. Solids*, **352**, P. 3608 (2006).
[19] Xu Huibing, Zhuang Weidong, Wen Xiaofan, Liu Ronghui, Hu Yunsheng, Xia Tian, Effect of Li^+ ions doping on structure and luminescence of (Y,Gd)BO_3:Tb^{3+}. *J.Rare Earths*, **28**, P. 701 (2010).
[20] Liu Bingjie, Gu Mu, Liu Xiaolin, Zhang Rui, Xiao Lihong. Effects of Li^+ and Zn^{2+} Co-doping luminescent properties of Gd_2O_3:Eu^{3+} nanoparticles. *J.Rare Earths*, **25**(2), P. 164 (2007).
[21] Yu Zhijian, Huang Xiaowei, Zhuang Weidong, Cui Xiangzhong, He Huaqiang, Li Hongwei. Co-precipitation preparation and luminescent behavior of (Y,Gd)BO_3:Eu phosphor. *J.Rare Earths*, **22**, P. 829 (2004).
[22] Bachir S., Azuma K., Kossanyi J., Valat P., J. C. Ronfard-Haret. Photoluminescence of polycrystalline zinc oxide co-activated with trivalent rare earth ions and lithium. Insertion of rare-earth ions into zinc oxide *J.Lumin.*, **75**, P. 35–49 (1997).